Measurement 182 (2021) 109759

Contents lists available at ScienceDirect

Measurement

journal homepage: www.elsevier.com/locate/measurement

An enhanced indirect video-based measurement procedure for dynamic structural system identification applications

Mehdi Ghandil [a], Ömer Dabanli [b], Hossein Tajmir Riahi [a,*]

[a] Department of Civil Engineering, University of Isfahan, Iran
[b] Research Center for Conservation of Cultural Heritage, Department of Architecture, Faculty of Architecture and Design, Fatih Sultan Mehmet Vakif University, Turkey

ARTICLE INFO

Keywords:
Structural dynamic identification
Video-based indirect measurements
Virtual visual sensors
Magnification
Digital signal and image processing

ABSTRACT

A video-based indirect sensing procedure for dynamic identification purposes is presented. To overcome major limitations of video-based methods in real on-site measurements, a novel three step pre-modification, magnification, post-modification process is developed. This process includes revision of the initial input video record in order to delete disturbing objects, utilizing a magnification method to filter the frequency content of the monitored motion and using a revision step for elimination of noises generated during magnification process. Finally, a set of digital signal and image processing analyses are performed on the modified video using virtual visual sensor technology. Based on the results of this research, motion signals of the monitored object are detected. The proposed approach has been used for identification of dynamic characteristics of two historic masonry minarets in Istanbul. Results shows that the proposed procedure is able to assess the dynamic characteristics of the monitored structure with a high-level of accuracy.

1. Introduction

Civil engineering structures are permanently under environmental low-amplitude vibrations. The vehicles traffic, daily winds and even walking pedestrians around these structures are the usual sources of these existing ambient motions [1,2]. However, the vibrations can be used for the structural dynamic system identification procedure. Consequently, dynamic parameters and possible damages of the structure can be investigated and/or identified by interpretation and signal processing of the ambient data. The ambient motions of a monitored structure can be measured using direct (contact) and indirect (non-contact) methods. In the direct contact method, the physical sensor networks are used to record motions of the structure. Usual or new high-tech equipment such as wireless or wired accelerometers, strain gauges, LVDTs and GPS technologies are now utilized in this regard [3–6]. In contrast, novel indirect measurement technologies do not require such contact elements. From cameras to unmanned aerial vehicles and scanning laser vibrometry, the efficiency and performance of various types of instruments have been examined in these technologies [7]. Camera-based structural health monitoring depending on virtual visual sensors (VVSs) is one of these modern methods. Some technical procedures related in this subject, such as vibration-based monitoring especially for historical buildings and Eulerian video magnification, are briefly reviewed at the following.

Vibration-based dynamic system identification process has been performed in historical buildings and sufficient results and experiences have been obtained [8–12]. This process was also examined for bridges [13–19], buildings [11,20–25] and tall towers [26–32]. This method is more effective for bridge structures, due to their considerable permanent ambient vibrations [18,19]. Also, the historical tall towers such as minarets and bell towers are appropriate cases for investigation using this method because they have a high level of structural height and consequently strong vibrations during daily ambient excitations.

The video-based measurement procedures are indirect and contactless technologies that can be promisingly applicable in structural system identification and health monitoring subjects. An ideal environmental and good weather conditions during video recording are the essential requirements for their efficiency and accuracy. These conditions are not usually observed in real SHM projects. Consequently, the application of such procedures can face serious limitations. The video-based procedures have been investigated for structural system identification of civil infrastructures in several research works. The main purpose of these researches is identification of natural vibration characteristics using remote video-based measurement techniques [33–49]. Both of low-

* Corresponding author.
E-mail address: tajmir@eng.ui.ac.ir (H. Tajmir Riahi).

https://doi.org/10.1016/j.measurement.2021.109759
Received 12 March 2021; Received in revised form 14 May 2021; Accepted 11 June 2021
Available online 19 June 2021

quality equipments and high and super-high frame-rate cameras have been separately examined in structural system identification studies. From their results, it was not observed that using expensive equipments and high-speed cameras are effective in minimization the level of noises and improvement of the motion signal quality [50]. But, it is found that the use of some video modification techniques such as Eulerian video magnification (EVM) procedure can be effective in increasing the signal-to-noise ratio [51].

The EVM is a new technique developed for revealing temporal variations in videos that are difficult or impossible to be detected with naked eyes [42]. In this method, a standard input video sequence is spatially decomposed by applying temporal filters on the video frames. The resulting signals are then amplified to detect possible small motions. As a main drawback of linear approach of EVM procedure, the undesirable noises are amplified as well as target small motions. In order to overcome this limitation, the phase based motion processing has been developed [40]. According to the basis of this method, only variation signals are amplified that their frequency content falls within a specific frequency bandwidth [41,52]. In another research, a motion magnification method using spatio-temporal filtering and image warping was presented in order to improve the EVM procedure and provide a better post-processing way to handle the frame noises [37]. Liu et al. [53] amplified subtle motions accurately by Lagrangian analyzed feature point paths. Elgharib et al. [36] combined both Eulerian and Lagrangian approaches and tried to magnify small motions to higher-levels of motion amplitudes. Zhang et al. [44] tried to enhance the procedure performance by magnifying accelerations instead of displacements.

In the reviewed related studies, the field-measurement process has been conducted in not crowded physical environments, under good sun and weather conditions and also with presence of a single moving object. In the other studies, the video recording step has been performed in controlled experimental conditions. The real-time monitoring projects are often not faced to such good situations. Usually, one or more stationary or moving disturbing object is present next to the monitored object in the background or forefront of the video frame. Refraction in the air layers under inappropriate weather conditions like wind, storm or rain can also criticized the measurement process. In such cases, both of the magnification and digital signal processing procedures lead to low-accuracy results with high-level of occurred noises. Therefore, the use of inappropriate input video records under real conditions is inevitable. Instead, such motion records can be converted to idealized videos containing only target motion of the distinct monitored object having sharp and clear boundaries with presence of simple one-color background and absence of any other disturbing objects.

The main contribution of this study is presentation of an effective and low-cost indirect measurement procedure including a video conversion process to develop the application of these technologies to real-time structural health monitoring projects. The motion videos, recorded by simple and low-quality cameras or in overcrowded physical environments; or including disturbing extra moving objects are good candidates as input data for this process. The proposed procedure is based on a three step video conversion process including pre-modification, magnification and post-modification (PMP) steps in order to revise the motion video records facing undesirable conditions. At the first step, in order to make the subsequent video processing steps faster with less data size on disk, the recorded video resolution can be reduced. Then, possible disturbing objects are eliminated using video editing techniques, in such a way that the video includes only the monitored object as a single moving element with sharp and distinct edges. The output video is magnified to filter its frequency content in the second step. The third step is applied to reduce generated noises and unknown pulse during magnification. The final modified motion video record is used for digital signal and image processing using virtual visual sensor (VVS) technology.

Two key-point and region-based approaches can be utilized in the VVS-based signal processing. The first approach extracts the motion signal of the accurate target point from its corresponded pixel as the key-point. In the second approach, in addition to the key-point pixel, its neighbor pixels are contributed in the signal processing and an averaged motion data are extracted. The related details are described in the methodology of the proposed procedure. Additionally, in order to investigate its efficiency and accuracy in real and unpleasant weather conditions, this study is accompanied by presentation of an example of application. The procedure has no limitation on type and structural features of the monitored object. It also doesn't require input motion video records with high-resolutions or large sizes. Since no comprehensive research has been done using video-based indirect measurements in historical buildings such as mosques and their minarets, this research investigates these interesting structures as the intended example of application. Accordingly, two minarets of Nur-u Osmaniye Mosque in Istanbul are selected for the investigation. From the field-measurements, the motion signals are extracted and analyzed. Consequently, the experimental modal characteristics (such as two first modal frequencies and damping ratios) can be detected. Also, by using these signals, the time history responses at the top point of the minarets are obtained. The results are verified by comparison with output signals measured by an accelerometer sensor as a conventional measurement method.

2. The proposed video-based indirect measurement methodology

The procedure intended in this study has four major steps: a) The real-time on-site video recording; b) PMP processing; c) VVS-based digital signal and image processing; and d) Time history response calculating. An overview implementation chart of the procedure is presented in Fig. 1. The presented steps in the figure are discussed in the following.

2.1. Real-time video recording

The first video recording step can be conventionally conducted using simple and low-cost cameras. The selection of a suitable camera position in such a way that directly includes the monitoring object is necessary. The camera must be fixed in its position using for example a tripod statically mounted on the base. The locations of these items should be accurately addressed in a site plan drawing. Also, it is necessary that the camera inclination angle from the horizon in elevation view is measured during video recording.

2.2. PMP processing

This video conversion process is developed for preparation of input video records especially in real-time monitoring progresses having inappropriate environmental and unpleasant weather conditions. The three sub-steps of this process shown in Fig. 1 are briefly discussed in the following.

2.2.1. Pre-modification of input video record

In the proposed procedure, input video records with crowded contents can be effectively revised by applying two modification steps before and after of the magnification. The first modification includes video editing techniques such as rotation, crop, zoom and increasing the video contrast value to maximum level by means of existing commercial software package. If needed, the initial resolution of the video record can be reduced. This modification eliminates disturbing objects and sharpens the boundary of the monitored object.

2.2.2. Magnification process

A middle sub-step magnification is considered between two intended magnifications in order to filter the monitored motion frequency content of undesirable pulses and other possible motions. This process is con-

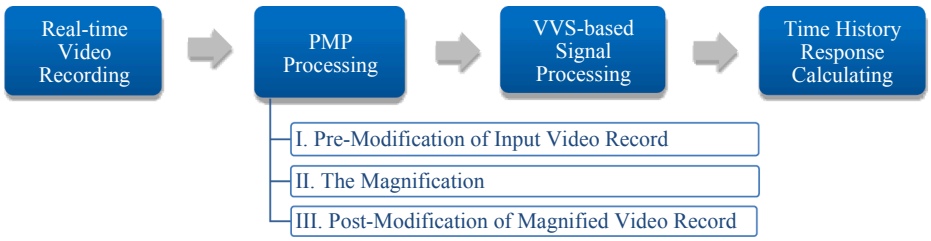

Fig. 1. The overview of the proposed video-based indirect measurement.

ducted using phase-based Eulerian Video Magnification (EVM) method recommended for small motions [40]. In the following, a brief overview of EVM theoretical basics is presented. During propagation of a small signal due to a one dimensional small motion, if the color function at initial position of x_0 is determined as $I(x_0,t)$, the subsequent location and function value after a time step of $\delta(t)$ are $x = x_0 + \delta(t)$ and $I(x,t) = f(x+\delta(t))$, respectively (with the initial condition of $I(x,0) = f(x)$). The color function after the magnification of its motion signal with α-factor is [42]:

$$\widehat{I}(x,t) = f(x + (1+\alpha)\delta(t)) \tag{1}$$

The result of its equivalent Taylor series is:

$$I(x,t) = f(x) + \delta(t)\frac{\partial f(x)}{\partial x} \tag{2}$$

Now, if a filter function as $B(x,t)$ is applied on the color function in such a way that be effective on everything except $f(x)$, then $B(x,t) = \delta(t)\frac{\partial f(x)}{\partial x}$ and the filtered color function changed into:

$$I(x,t) = I(x,t) + \alpha B(x,t) \approx f(x) + (1+\alpha)\delta(t)\frac{\partial f(x)}{\partial x} \approx f(x + (1+\alpha)\delta(t)) \tag{3}$$

According to this equation, the displacement function $\delta(t)$ at x position has been magnified by $(1+\alpha)$ times, applying filter of $B(x,t)$. As an example, a low-amplitude cosine wave as a black line has been magnified in Fig. 2. In this figure, the subsequent location of this wave before and after process is indicated in blue and red lines, respectively. According to this figure, the magnified red wave is clearer and more distinct than original displaced blue wave [42].

For implementation of this process, a developed MATLAB-based algorithm is used [42]. In addition to pre-described α, this algorithm utilizes three other major parameters as I_o^{cutoff}, h_i^{cutoff} and σ. The range of $\left\{I_o^{cutoff}, h_i^{cutoff}\right\}$ determines the cut-off frequency bandwidth. All motions having frequency values out of this range are not magnified and can be eliminated. In the other words, the process magnification is applied only on motions and vibrations having excitation frequencies falling within this frequency bandwidth. An iterative process is required to determine the upper and lower bounds of the bandwidth. This iterative process and all subsequent steps like digital signal & image processing described at the next section should be performed separately for frequency each mode.

A large enough value can be used for h_i^{cutoff} parameter as the considered upper bound frequency. This value can be approximately calculated from a numerical modal analysis of the monitored object. In this regard, it is not necessary to use any accurate data from physically installed sensors. The usage of accelerometers data is always an available option, but if the proposed procedure is taken into consideration as new and independent method, it should be able to work without any sensors. Therefore, in this study, the sensor data have been used only for verification in the final comparison step, not directly as input data in the indirect measurement.

The lower bound of the frequency bandwidth (I_o^{cutoff}) for each mode, should be equal to an appropriate value smaller than the upper bound in such a way that the bandwidth includes the experimental value of modal frequency. The factor of σ (in *pixel*) is used for reduction of undesirable noises generated in magnification process. As the higher value is considered for this parameter, the quality of magnified video is higher. But, it is necessary to note that the use of large amounts for σ causes the magnification effects to be eliminated [40]. The appropriate values of α and σ factors should be iteratively assessed.

2.2.3. Post-modification of magnified video records

Magnified videos usually are accompanied by generated noises and waves around the monitored moving object [40]. In order to obtain accurate and high-quality output signals, another modification step is considered to apply on the magnified video. In this modification, the video is binarized to a B/W (black/white) image mode by increasing the video contrast value to an adequate level. As a result, the magnification generated waves are removed and the video quality is improved.

2.3. VVS-based digital signal & image processing

The main purpose of digital signal processing on the motion video records is detection and extraction of motion signals from specific

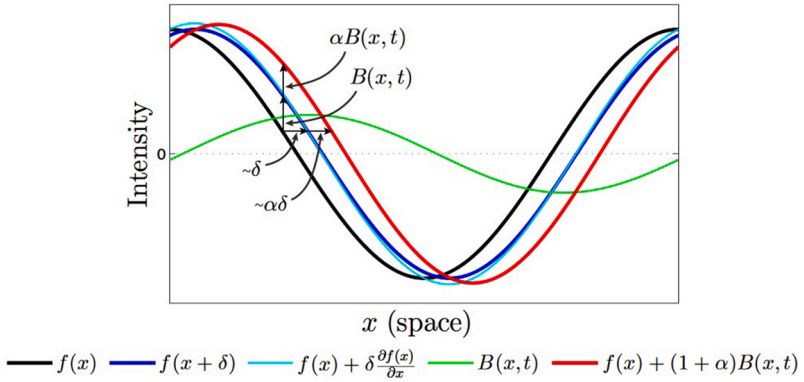

Fig. 2. The effect of EVM process on a f(x) cosine wave [42].

selected pixels placed on the edge, boundary or corner of the monitored vibrating object. The motion signals can be directly extracted from the initial video record without any magnification. However, in this section, it is shown that the implementation of the magnification procedure leads to clearer frequency content with less noises. In video-based dynamic system identification procedures, the mentioned pixels are considered as virtual visual sensors [54]. The term "VVS" follows the terminology presented by Song et al. [55]. This methodology that its concept has been shown in Fig. 3, uses an Eulerian specification where a specific pixel on the structural boundary is selected and monitored in grey-scale mode. Since the color mode of the input video had been changed to B/W before, the brightness of the selected pixel at location x_p and $y_p$can be high-accurately monitored over time. Consequently, the output time history data can also be analyzed using the Fast Fourier Transform (FFT) to reveal the high-amplitude peak pulses at modal frequency values (Fig. 3) [56,57].

In this procedure, the mentioned monitoring process of the pixel is conducted using a MATLAB code developed by the authors using Lucas-Kanade Optical Flow Algorithm [59–62]. The concept of Optical Flow is based on pixel brightness constancy assumption. If $B(x_0, y_0, 0)$ is considered as brightness function of the monitored pixel with initial spatiotemporal position on the first video frame, $B(x_i, y_i, t_i)$ represents its transferred position in the current frame, in which $x_i = x_0 + \Delta x_i$, $y_i = y_0 + \Delta y_i$ and $t_i = 0 + \Delta t_i = \Delta t_i$ (Δt_i is equal to $(i-1)dt$ in which, dt is constant in throughout of the video record). The constant top-left corner of the video frame is considered as origin of coordinates for all pixels. The mentioned constancy assumption leads to:

$$\mathrm{B}(\mathrm{x}_0, \mathrm{y}_0, 0) = \mathrm{B}(\mathrm{x}_\mathrm{i}, \mathrm{y}_\mathrm{i}, \mathrm{t}_\mathrm{i}) = \mathrm{B}(\mathrm{x}_0 + \Delta \mathrm{x}_\mathrm{i}, \mathrm{y}_0 + \Delta \mathrm{y}_\mathrm{i}, \Delta \mathrm{t}_\mathrm{i}) \tag{4}$$

The right-hand side of the above equation can be rewritten as its equivalent Taylor series form. Thus:

$$\begin{aligned} B(x_0, y_0, 0) &= B(x_0 + \Delta x_i, y_0 + \Delta y_i, \Delta t_i) \\ &= B(x_0, y_0, 0) + \frac{\partial B}{\partial x_i}\Delta x_i + \frac{\partial B}{\partial y_i}\Delta y_i + \frac{\partial B}{\partial t_i}\Delta t_i \rightarrow \frac{\partial B}{\partial x_i}\Delta x_i + \frac{\partial B}{\partial y_i}\Delta y_i + \frac{\partial B}{\partial t_i}\Delta t_i \\ &= 0 \end{aligned} \tag{5}$$

The final equation can be rewritten as a simple form:

$$B_x\frac{\Delta x_i}{\Delta t_i} + B_y\frac{\Delta y_i}{\Delta t_i} + B_t = 0 or B_x V_{x_i} + B_y V_{y_i} + B_t = 0 \tag{6}$$

To determine the values of V_x and V_y unknowns from solving Eq. (6), two methods of Horn-Schunck and Lucas-Kanade have been proposed. In this research, the Lucas-Kanade method is used [62]. To solve this equation according to this method, the input video frame is divided into smaller regions with velocity constancy in each region. Then, a weighted least-square fit of Eq. (6) to a constant model for $\begin{bmatrix} V_{x_i} & V_{y_i} \end{bmatrix}^T$ in each region Ω is performed. The method achieves this fit by minimizing the following equation [61]:

$$\sum_{\text{pixels}\in\Omega} W^2 \left[B_x V_{x_i} + B_y V_{y_i} + B_t\right]^2 \tag{7}$$

W is a window function that emphasizes the consistency at the center of each zone. The solution to the minimization problem is:

$$\begin{bmatrix} \sum W^2 B_x^2 & \sum W^2 B_x B_y \\ \sum W^2 B_y B_x & \sum W^2 B_y^2 \end{bmatrix} \begin{bmatrix} V_{x_i} \\ V_{y_i} \end{bmatrix} = -\begin{bmatrix} \sum W^2 B_x B_t \\ \sum W^2 B_y B_t \end{bmatrix} \tag{8}$$

For the real solution of the above equation, it is necessary that the determinant of the coefficient matrix is nonzero. Otherwise, the solution leads to "NaN" answer for V_{x_i} and V_{y_i} values. These values can be considered as the time history data of velocity record (in *pixel*/*s*) for the monitored pixel [62]. Consequently, the time history of displacement response with along horizontal *x*-axis or vertical *y*-axis to the measured ambient vibration can be calculated according to the below equation:

$$\begin{aligned} U_{x_i} &= V_{x_i} dt + U_{x_{i-1}} \\ U_{y_i} &= V_{y_i} dt + U_{y_{i-1}} \end{aligned} \quad (i = 1, 2, \cdots, NF) \tag{9}$$

In this equation, U_{x_i} and U_{y_i} are the horizontal and vertical displacements of the monitored moving pixel on the i^{th} video frame at $t = t_i = i \times dt$, respectively. dt is the length of each time step equal to $1/F_r$ (F_r is the video frame rate or camera sampling frequency). NF is the number of video frames in the record. Since there is no 0^{th} frame in the record (this frame can be assumed as an initial black frame), it is considered that $U_{x_0} = U_{y_0} = 0$. These results can be drown as true structural displacement time history response after applying some other corrections discussed in the next section.

This monitored pixel can be selected in any place on the video frame without any limitation, but the preferred location is usually on the edge, boundary or corner of the vibrating target object as the key-point pixel. Depending on contribution of the surrounding pixels, the VVS-based signal processing can be performed as two major Key-Point matching and Region-Based matching approaches. In the first approach, only the target pixel as considered as the key-point for detection of the motion signals. In the second approach, a $(2n+1)$ *pixel* $\times$ $(2n+1)$ *pixel* square region around the key-point pixel can be considered. An averaged motion signal corresponded in overall to the square region is calculated as the major output of this approach. In order to select appropriate values for *n*-parameter, a set of sensitivity analyses should be performed on the object video record considering various values of this parameter. The case in which the smoothest frequency spectrum with lowest noises is obtained, can be considered as an appropriate *n*-value.

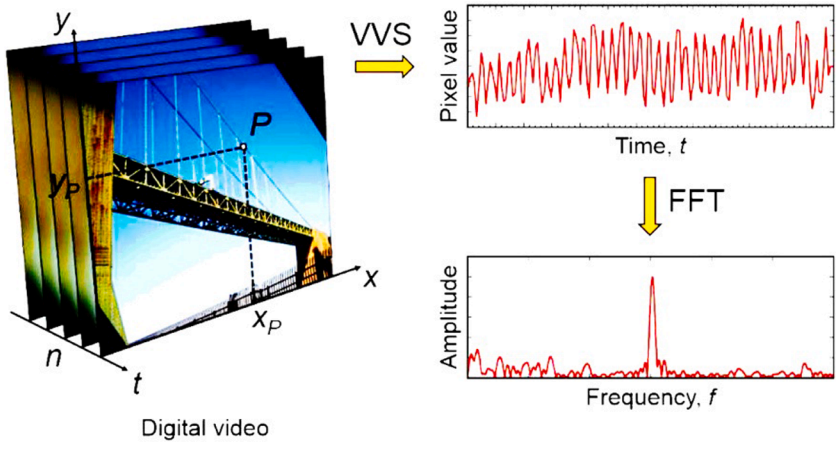

Fig. 3. The concept of virtual visual sensor (VVS) methodology [58].

2.4. Time history response calculation

For determination of the displacement time history response at the monitored pixel, it is necessary that four corrections are applied on the results of Eq. (9). These required corrections are described in the following.

2.4.1. Unit conversion and perspective effect

The first one is the unit conversion factor (*UCF*). This factor converts the data unit from *pixel* to a desirable displacement unit (for example *mm*). The value of this factor should be determined from measurement of a same object's length in two actual and virtual environments as unit conversion criterion. Due to perspective effect, the *UCF* value is different in various positions on the video frame. Therefore, the mentioned object's length should be measured exactly in the position of the selected VVS point. If the full-monitored object has large geometrical dimensions in comparison to its average distance from the camera, the perspective effect is significant.

2.4.2. Camera position angle

The second correction is related to camera position angle. In some monitoring procedures due to place limitations, it is possible that the camera is placed in such a way that its lens axis may not be normal to the motion direction. This situation affects the horizontal component of the monitored motion. For example, Fig. 4 presents the plan view of a tubular structure under horizontal vibration. According to this figure, the angle between camera axis and horizontal motion normal axis (θ_p) is consedered as camera position angle and the extracted motion signal needs to be divided by $\cos\theta_p$.

2.4.3. Camera inclination angle

Another correction is related to camera inclination from ground level. This situation can be occurred when the Camera placed on the ground is recording a vertical motion at a high-altitude. This situation affects the vertical motion component. For example, Fig. 5 presents the square section of a beam under vertical vibration in side view. In this recording case, the camera inclination angle (shown as θ_i in the figure) affects the detected vertical signal motion. Therefore, the signal data should be divided on $\cos\theta_i$.

2.4.4. Magnification effect

The final correction is related to the conducted magnification process and its α-factor. As discussed, the magnification process amplify the monitored motion and shifts its frequency content to a range that excludes the other undesirable motions and noises [40]. This factor practically has a nonlinear and complex effect on the output signal amplitude. As the value of this factor is increased, the difference between two amplified and true signals is higher. Therefore in order to identify the true motion amplitude, it is necessary that the magnified output signal is scaled in such a way that its amplitude is not greater than the amplitude of true signal. This true signal amplitude should be indirectly determined. For this purpose, an iterative sensitivity analysis is necessary considering various large enough values for α-factor. As a convergence criterion, FFT curves including the same modal peak frequency should be observed at the end the iterations. Thus, the trend of

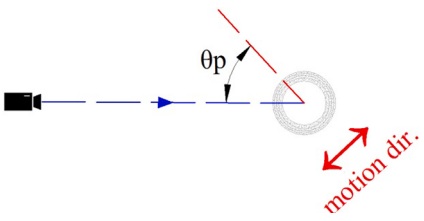

Fig. 4. The camera position angle (θ_p) in recording of a horizontal motion.

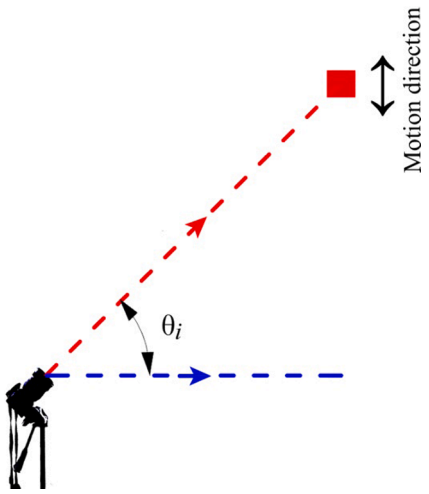

Fig. 5. The camera inclination angle (θ_i) in recording of a vertical motion.

motion signal amplitude in comparison of α variations can be determined. The results can be drawn as consecutive discrete iteration points with a fitting curve in a graph similar to Fig. 6.

A general relationship between signal amplitude and α has been shown in Fig. 6. For small α values in the region of strong noises, the magnification process is not powerful enough to eliminate them. For larger α values, the better results with weak noises can be obtained. The extra larger values for this factor may lead to mitigated motions [40]. If the iteration points fall within the range of optimized α values, the vertical intercept of their fitting curve (D_0) can be an acceptable approximation as the true signal amplitude. Accordingly, the amplitude scale factor (*ASF*) is defined as:

$$ASF = \frac{D_i}{D_0} \tag{10}$$

In this equation, D_i is the magnified signal amplitude in the preferred iteration. Finally, all four described corrections are applied on the magnified signal according to the below equation:

$$U_i = \frac{UCF \times U_i}{ASF \times \cos\theta_p \times \cos\theta_i} \tag{11}$$

In which, U_i is the horizontal or vertical component from Eq. (9). U_i is the corrected time history displacement response in the same direction under real-time measured ambient excitation.

3. Example of application: minaret structures

The methodology of the proposed indirect camera-based procedure

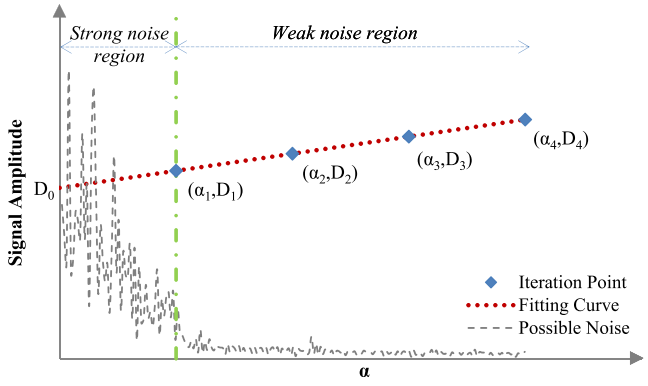

Fig. 6. The general trend of motion signal amplitude in variation of α.

has been reviewed in Section 2. In this section, its application in real-time monitoring projects is investigated. At first, a comparison about structural features and monitoring requirements between these kinds of historical buildings and ordinary infrastructures such as bridges and residential buildings is briefly disscussed here.

Generally, minarets as long and slender structures are more vulnerable against lateral loads such as earthquakes and winds than vertical loads. Nevertheless, unlike modern engineering structures (bridges and buildings), there is no standard or guideline for analysis and design of the minarets. The cracks and possible damages on the minaret body may occur depending on some external factors. For example, the material strength of the cylindrical body may be decreased. Conversely, the material strength of the internal stairs can be decreased less. Accordingly, stairs have important role in the structural behavior of the minarets. In general, the structural analysis of minaret structures are usually more complicated and accompanied by more difficulties (due to existence of stairs and uniform mass distribution) than ordinary infrastructures like building frames. In SHM projects, the efficiency of this proposed indirect measurement procedure is more prominent for towers such as minarets and bridges which are not easy for instrumentation and sensor network installation. This is the reason for selection of the minaret structures in this example of application. Two historic masonry minarets of Nur-u Osmaniye Mosque are investigated in this regard. The obtained results will be verified according to outputs of performed sensor-based direct measurement. In the next sub-sections, the conducted investigation is discussed step by step.

3.1. History and architecture

Nur-u Osmaniye Mosque, which was constructed between 1748 and 1755, is one of the most significant monuments of the capital of Ottoman Empire in Istanbul (Fig. 7). The mosque is located within the borders of Fatih district, on the northwest side of Çemberlitaş, near the area where famous East Rome period work Constantinus Forum, as a part of the Kulliye (Islamic Ottoman Social Complex). The mosque is known as the most significant representative of the new era in 18th century Istanbul and called as “Ottoman Baroque”.

Nur-u Osmaniye Mosque has a sanctuary place which rises on a classic square baldachin plan with 27.35 m axis and covered by a single central dome which is supported with four masonry main arches and the help of pendants on the corners of the sanctuary space. The elliptic courtyard of the mosque is covered with fourteen small domes [63].

3.2. Structural system and material

The load-bearing system of the mosque is also very simple. Masonry walls of main sanctuary space, pillars and arches both in the courtyard and minarets, were constructed with cut stone technique and made of limestone, an organic stone type named as kufeki, which is commonly used in Ottoman Monuments of Istanbul. The structural elements were built with hammer-dressed stone masonry technique and the metal instruments such as clamps, and mortises were used to connect each stone block to another. Furthermore, the structure was strengthened with iron tie beams on each nine levels during the construction. In sanctuary and courtyard of the mosque, there are marble and granite columns supporting the gallery floor and brick domes of portico. The height of the main dome which was built with traditional bricks and lime (Khorasan) mortar is approximately 42 m from ground floor to the top [63,64].

The mosque has two minarets which were constructed cut limestone stone and elevated on a square marble pedestal that is united with the walls of the sanctuary and the courtyard up to the dome level of the portico (Figs. 8 and 9). After this level, the minarets rising in the form of cylindrical towers independent of the structure of the mosque. There are two balconies in the minarets, which have identical features. The circular stairs reach to the second balcony level inside the minarets. The spires which were wooden in the first construction and after several fires and damages they were replaced with natural stone.

Minarets have rectangular bases with 4.2 m × 5.4 m dimensions in plan and 12.1 m in height. Above the 12.1 m high base which is connected with the walls of courtyard and mosque, the minarets narrow along the 4.5 m height of the cube section and become a circular planned tower. The outer and inner diameter of cylindrical body is 2.75 m and of 1.65 m, respectively. There are spiral stairs which reaches two balconies along the minarets. The total net height of the minaret rising independently from the mosque after the base is 47.5 m including the spire and the total height of minarets including basement part from the ground floor level is 59.6 m.

3.3. Instrumentation and data acquisition

Minarets are most vulnerable parts of historical mosques. Therefore, a regular inspection, system identification and SHM process is required

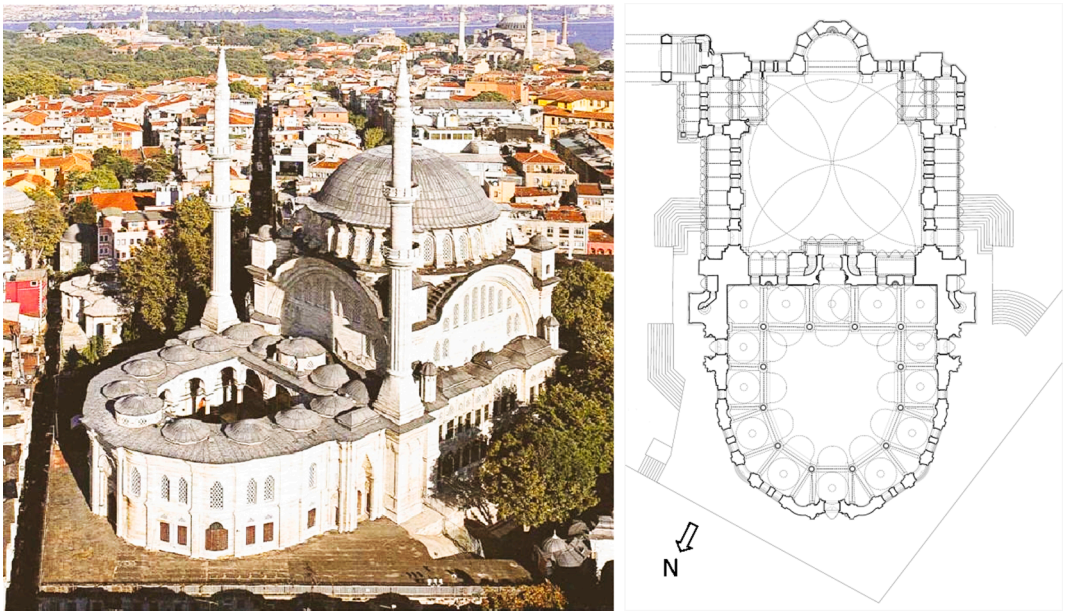

Fig. 7. Nur-u Osmaniye Mosque, photograph from west (C. Emden) and plan layout [63].

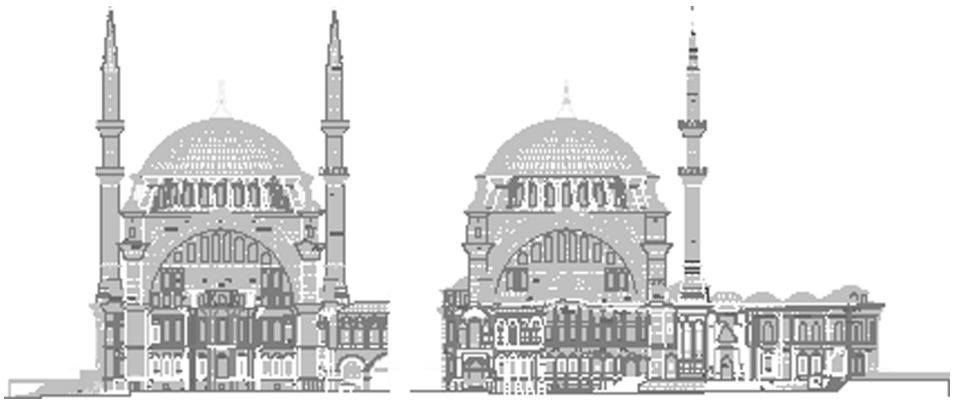

Fig. 8. South-east (Qibla) and North-east façade of the mosque [63].

Fig. 9. General views of the minarets [63].

for these sensitive historic structures. For this purpose, both minarets of Nur-u Osmaniye Mosque which is an 18th century Ottoman monument in Istanbul have been selected for this investigation.

In this study, the first data were collected with accelerometer. Generally, the appropriate positions for accelerometers and installation of devices can be found at balcony level in the minarets. An accelerometer was installed at the second balcony level of each minaret for data acquisition in order to compare and verify the results of the purposed indirect VVS-based method. Operational modal analysis on minarets were performed with a triaxial force-balance type *Güralp System CMG-5TD Digital Accelerometer* (0.01 g sensitivity) and computer (Fig. 10). The ambient vibration data recorded for fifteen minutes with sampling rates equal to 200 Hz.

The second setup for data recording of the minarets was performed with a *Nikon D5300* single-lens reflex digital camera shown in Fig. 11. The camera has video output of NTSC & PAL standards with .MOV file format; H.264/MPEG-4 advanced video coding; data rate of 54 *Mbps*; dimensions (W × H × D) of approx. 125 × 98 × 76 mm and total weight

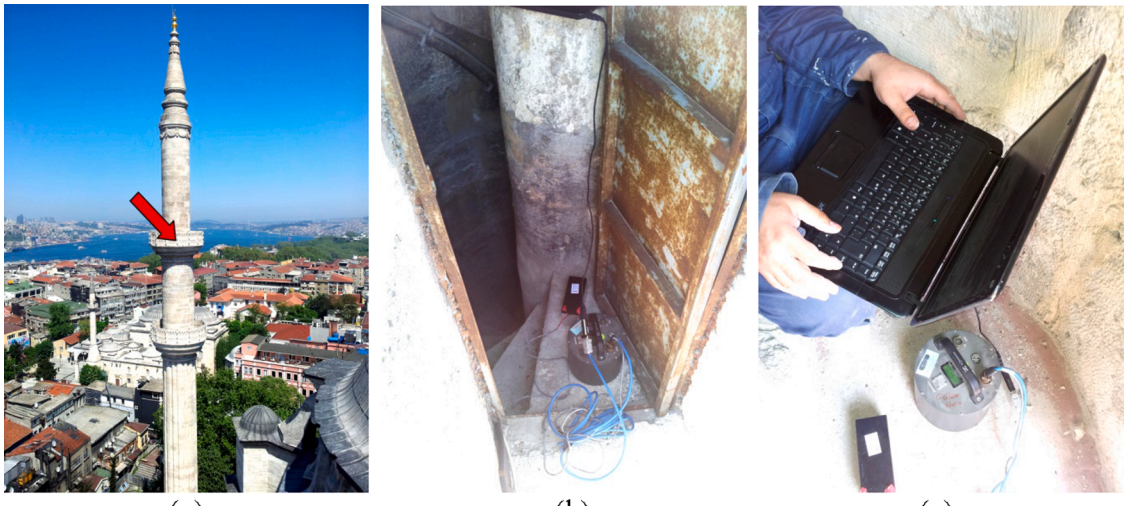

Fig. 10. General views of minarets, a-b) device location c) data acquisition equipment.

Fig. 11. The *Nikon D5300* digital camera used for video recording of the minarets.

of approx. 530 g, as its major technical specifications. It was fixed on a tripod statically mounted on the ground surface. In order to examine the efficiency and accuracy of the proposed indirect measurement procedure under unpleasant weather conditions, the video recording step was conducted in a windy and rainy day. For detection the wind direction more accurately, it was also checked out based on the meteorological data [65]. In Figs. 12 and 13, the camera positions on the courtyard plan and the views of the investigated minarets are presented, respectively. According to Fig. 12, four camera view (including two positions and two axes of 1 and 2 with the presented angles from qibla (south-east) direction have been considered at both locations inside and outside of the mosque courtyard. The selected camera positions have been arranged in such a way that the axes 1 and 2 are corresponded to the dominant wind direction for minarets 2 and 1, respectively. These two axes perpendicular to each other are corresponded to two first vibration modes of the minarets. The third mode is torsional and requires aerial video recording from above of each minaret to be detected. Accordingly, the two first experimental modes are investigated. For the camera views, the duration of each video record is two minutes, the recording frame-rate is equal to 59.94 fps. This equipment provides a frequency bandwidth with the range of 0–30 Hz. This frequency range is enough for detection of intended experimental modal characteristics in this example. Also, the resolution of the videos is 1920*p* to 1080*p*.

3.4. PMP processing

In this section, according to three sub-steps of the reviewed PMP processing, the preparation of the minarets video records is presented. For the pre-modification, three major video editing techniques have been used including rotation and crop corrections and the third, increasing the video contrast value to maximum level (herein 100%). The results of these corrections on the video records have been presented in Fig. 14. As these figures show, due to this modification, the additional elements (such as walls, mosque body, the sky and clouds) have been eliminated and also the skew of the minarets has been resolved. In this example, the recorded videos had initial resolution equal to 1920*p* × 1080*p*. Since there is not required that such a high-level of resolution is used in the proposed measurement procedure, these values can be reduced. After applying the mentioned corrections and reduction of the sizes of the videos, the final resolutions were obtained equal to 328*p* × 784*p*, 192*p* × 280*p*, 128*p* × 456*p* and 176*p* × 336*p* for the cases presented in Fig. 14 from top to bottom, respectively.

Also, the modified input video records with 5 s duration have been prepared and converted to AVI format with the same initial recording frame-rate (59.94 fps). The videos finally have been compressed using *IBM Motion JPEG video codec* recommended by the MIT researchers for the magnification process [40].

For the magnification process, a MATLAB code is developed according to the based-on phase-based method introduced in Section 2.2.2. At first, the natural frequency of the minarets is approximately calculated equal to 1.0 *Hz* from numerical modal analysis results of a simple cantilever column model using SAP2000 software [66]. Although, 1.0 Hz value for the first modal frequency of the minarets is overestimated in comparison with 0.71 *Hz* as the first natural frequency of the minarets obtained from operational modal analysis based on ambient vibration data acquired with accelerometer, it can be used as an appropriate value for h_i^{cutoff} parameter. Also after performing some iteration, it was observed that $I_o^{cutoff} = 0.6$ Hz is appropriate for the lower bound of the frequency bandwidth in this example. After an iterative process, it was observed that $\alpha = 6000$ and $\sigma = 80$ *pixel* are appropriate for all intended cases.

Each minaret has two similar vibration modes due to structural symmetry in its plan. Therefore, the first two modal frequencies are approximately the same. These values can be detected based on the two mentioned camera axis 1 and 2 which are perpendicular to each other. The third vibration mode of the minarets is a torsional motion and cannot be identified from the considered camera views. Therefore, in this study, the investigation will be limited to the first two modes of the minarets.

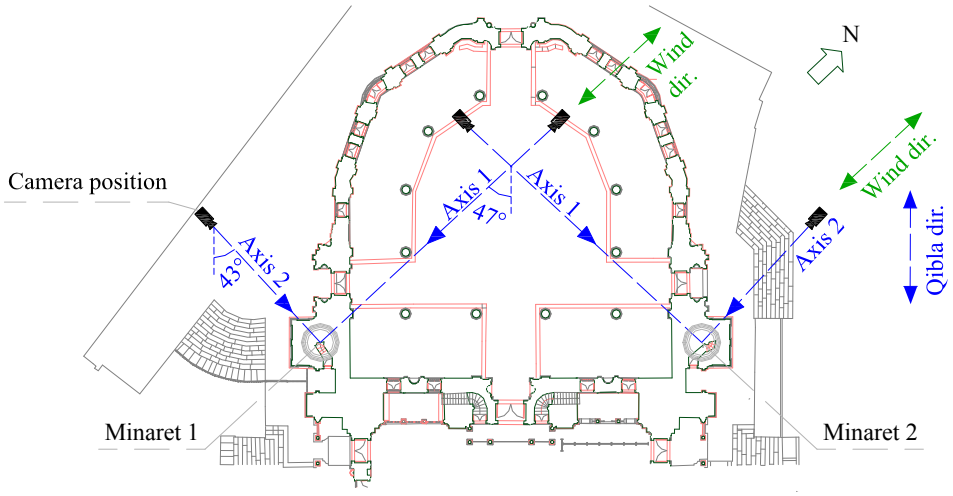

Fig. 12. The camera positions inside and outside of the courtyard.

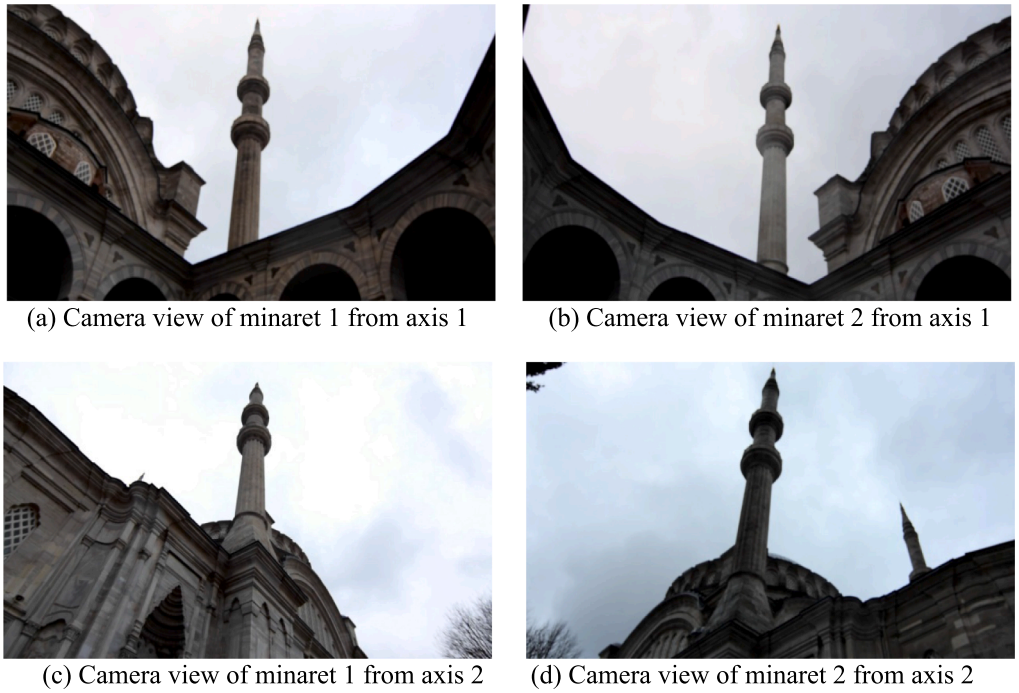

(a) Camera view of minaret 1 from axis 1 (b) Camera view of minaret 2 from axis 1

(c) Camera view of minaret 1 from axis 2 (d) Camera view of minaret 2 from axis 2

Fig. 13. The investigated minarets of the mosque.

In the post-modification step of the magnified videos, the video contrast value is increased again to maximum level (100%) in each case. The effectiveness and importance of the two pre- and post-modifications predicted in the proposed procedure are investigated here. The video record of minaret 1 with axis 1 camera view has been selected for this purpose. Three cases of magnification only (M), magnification with pre-modification (PM) and magnification with pre- and post-modifications (PMP) are considered for comparison. The observed results have been presented in Fig. 15. From this figure, it can be observed that the magnification process generates high-level of noises around the vibrating object (Fig. 15a). But the pre-modification step significantly reduces these noises (Fig. 15b). The best result is observed in Fig. 15c, in which both pre- and post-modification steps have been performed.

3.5. Digital signal processing of the records

The VVS-based digital signal processing according to the reviewed Lucas-Kanade Optical Flow algorithm is conducted using a MATLAB code developed by the authors. As mentioned before, this process can be performed using two key-point matching and region-based matching approaches. These approaches are investigated and their results are compared with each other in this example. Since the biggest probable motion can be expected to be occurred at the top level of the minarets under wind and other random daily excitations, the matched pixel on this position is selected as VVS A in each minaret. Also, the used accelerometer sensor in this study was installed at the second balcony of each minaret. Accordingly, the matched pixels in this position located on the boundaries at both left and right sides of the second balcony in each minaret are selected as VVS B and VVS C, respectively. Furthermore, a $(2n+1)$ *pixel* $\times$ $(2n+1)$ *pixel* square region around each VVS is considered in the cases for region-based matching approach. The positions of the VVSs including matched key-points and their surrounding square regions on the video record for the case of minaret 1 from axis view 1 have been illustrated in Fig. 16. The contents of this figure are generally similar to the other cases (which are not shown here for brevity). As can be observed from this figure, the origin of coordinate system has been located on the top left corner in each video frame. The considered values of n and obtained values of other geometrical parameters (based on the positions of the VVSs) shown in this figures are presented in Table 1 for all investigated cases.

In order to select appropriate values for n-parameter, a set of sensitivity analyses were performed on the minarets video records using region-based matching approaches. For each case, the value in which the smoothest frequency spectrum with lowest noises is obtained can be considered as an appropriate n-value. As an example, the case of minaret 2 video record along axis 1 (parallel to the wind direction) is investigated and the output frequency spectrum of VVS A has been presented in Fig. 17 for the case considering $n = 1$ to 4. In this figure (and the other similar figures in the following), each FFT spectrum is normalized to its maximum amplitude value.

According to Fig. 17, no significant difference can be observed in the frequency content of the spectra for different values of n. The peak pulse in all spectra was formed at the frequency of 0.7 Hz as a modal frequency value. However, the smoothest spectrum with lowest noises has been obtained for $n = 2$. Therefore, it is an appropriate value for this case. Similar sensitivity analyses were conducted for the other cases with their observed appropriate n-values given in Table 1.

Before discussing the results in the next section, the effectiveness of PMP process in noise reduction can be investigated here. Minaret 2 from axis view 2 is considered for comparison of detected VVS A motion signal in two cases of before and after PMP process applying. The resulted FFT spectra are presented in Fig. 18. These curves from initial and PMP modified video records have been labeled as “initial signal” and “PMP modifies signal”, respectively. The obtained first natural frequency of the minaret is equal to 0.70 Hz from accelerometer data and as can be observed, the frequency spectrum of the PMP modified motion signal is accompanied by the very low-amplitude noises compared to the initial ones. Also the first detected natural frequency of this case (0.70 Hz) is corresponded to the accelerometer output, unlike the other case (1.28 Hz) in which a significant difference can be observed.

3.6. Results and discussion

In this section, the main outputs of the proposed video-based procedure for the investigated minarets are discussed. The results include modal frequencies, damping ratios and time histories of displacement

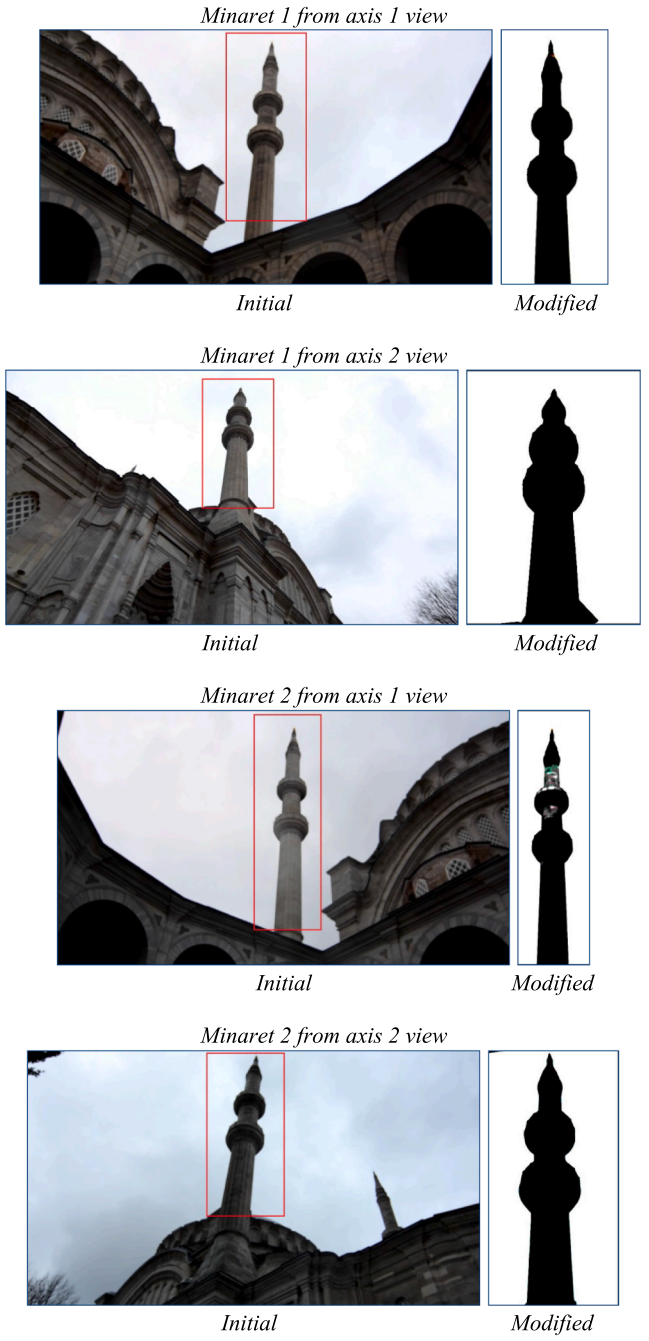

Fig. 14. The snapshot of the original and pre-modified video records of the minarets.

response at the selected VVS positions. Four cases including minarets 1 and 2 with the camera view from axes 1 and 2 are investigated with the label of $m-n$ in which, m and n indicate the number of the minaret and the axis of the camera view, respectively.

3.6.1. Modal frequencies

The FFT-based frequency spectra of the output motion signals are presented in Figs. 19 and 20 for 1-1 and 1-2 cases. For minaret 2, the results are similar and are not shown here due to brevity. The presented FFTs belong to two view axes perpendicular to each other and accordingly, they are corresponded to the first and second experimental modal frequencies. From these figures (minaret 1), it is clear that all the three selected VVSs located on the boundaries can similarly predict the modal characteristics of the monitored motions. The indirect VVS method is able to detect the modal frequency of the minarets with a very high-level of accuracy in comparison of the accelerometer data. Also, no meaningful and significant difference can be observed between FFT outputs of the two investigated indirect key-point and region-based approaches. These observations can also be confirmed for minaret 2.

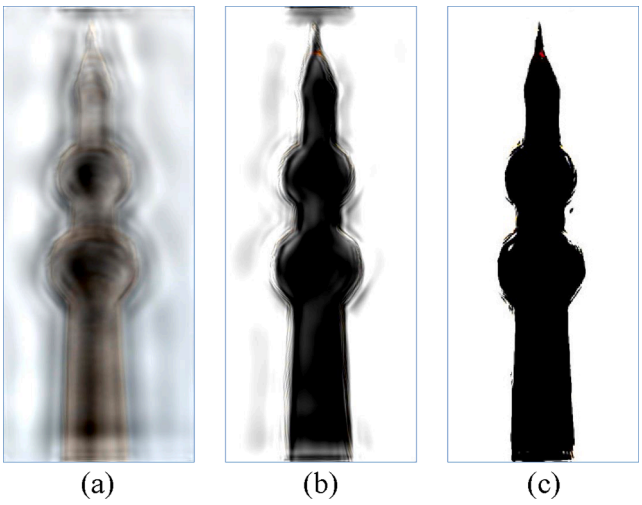

Fig. 15. A simultaneous snapshots of the minaret 1 video record from axis 1 in three cases of (a) M; (b) PM; and (c) PMP.

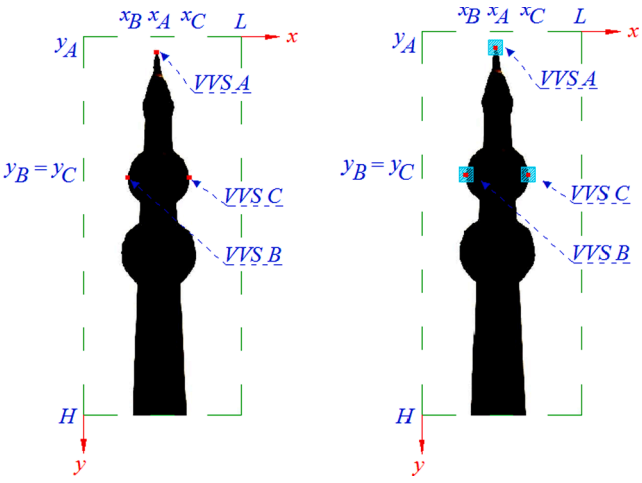

Fig. 16. The geometrical positions of the selected VVSs on the video record of minaret 1 from axis view 1 for both approaches.

Table 1
The values of n and other geometrical parameters of Fig. 15 for all investigated cases.

Parameter Value (pixel)	*Minaret - Axis View*			
	1-1	1-2	2-1	2-2
x_A	152	98	64	82
y_A	31	20	33	3
x_B	91	62	29	47
y_B	287	131	165	115
x_C	220	131	91	117
y_C	287	131	165	115
L	328	192	128	176
H	784	280	456	336
n	3	3	2	1

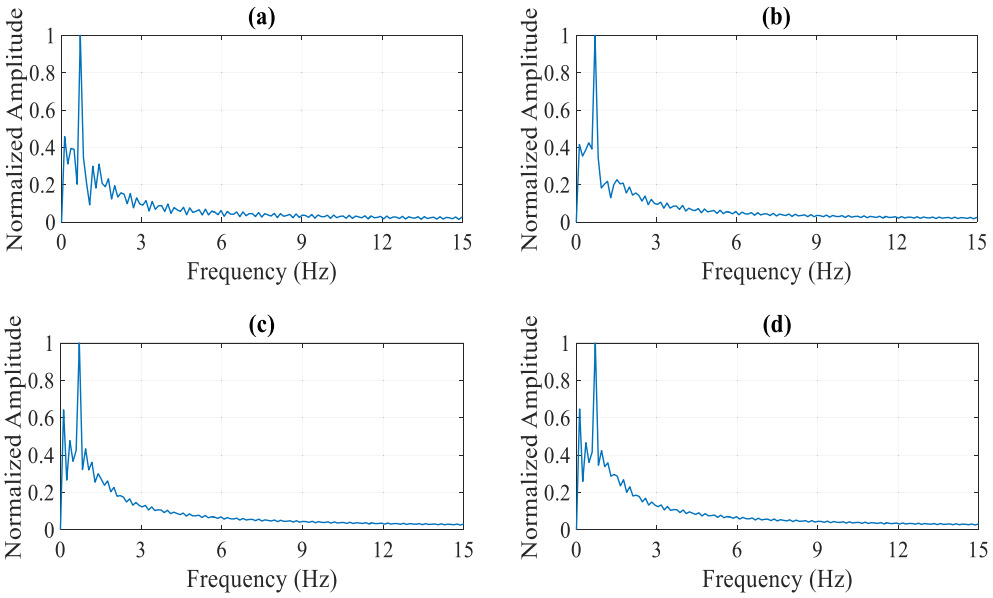

Fig. 17. The frequency spectra of the VVS A output motion signal in case 2-1 using region-based matching approach considering a) $n = 1$, b) $n = 2$, c) $n = 3$ and d) $n = 4$.

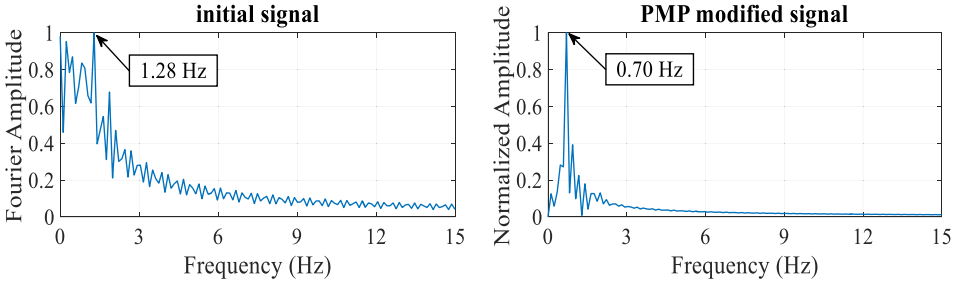

Fig. 18. The FFT spectra of VVS A motion signal for minaret 2 from axis 2.

3.6.2. Damping ratios

The experimental damping ratios of the minarets are determined from the FFT curves of the extracted motion signal presented in the previous section. For this purpose, the half-power bandwidth method is used [67]. According to the method, if A is the amplitude of the frequency spectrum at resonance position (f_r = resonance frequency), there is a frequency range with the name of "half-power bandwidth" in which, the lower and upper frequencies (f_a and f_b) have the same FFT amplitude equal to $A/\sqrt{2}$. Thus, the value of damping ratio can be determined as follows:

$$\xi = \frac{f_b - f_a}{2f_r} \tag{12}$$

The experimental damping ratios (ξ^{exp}) have been determined and presented in Table 2 for the first mode according to Eq. (1) and the calculated frequency spectra. From Table 2, the selected VVSs can be more accurately predicted the experimental damping ratio using key-point matching approach (KP) than the region-based approach (RB) in comparison with the accelerometer data. The average difference between VVS and accelerometer results are equal to 7.3% and 11.3% respectively for the key-point and region-based matching approaches.

3.6.3. Lateral drifts

As another main structural response, the lateral drifts calculated based on the detected time history records under ambient excitations, majorly winds around the minarets, is important to be discussed. The four corrections reviewed in Sections 2–4 are applied on the output signals. The details are as the following.

For the unit conversion factor, the external diameter of the minarets is considered for the required measurements. Since the minarets have large dimensions compared to the camera distance, the perspective effect is significant. This effect has been presented in Fig. 21b for minaret 1 from camera view corresponding axis 2. As this figure shows, the external diameter length (with the same true value equals to 2.5 m in height) is varying from 58 *pixels* at the bottom to 22 *pixels* at the top of the minaret due to perspective effect. Therefore, the value of *UCF* factor is different for the three monitored VVSs. The net height of the minaret and its horizontal distance to the camera position are 47.5 m and 13.9 m, respectively. In this situation, the value of *UCF* at the top, middle, and bottom of the minaret from this camera view is respectively equal to 114, 58 and 43 for conversion unit from pixel to mm. For both minarets and all camera positions, the values of this factor were calculated and applied on the extracted motion signals.

According to Fig. 12, both camera view axes are normal to their monitored motion directions (parallel and perpendicular to the wind direction). Thus no correction is necessary for the camera positions and $\theta_p = 0$ for all cases. Also, the camera inclination angles are equal to 65° (for the cases of 1-2 and 2-2) and 47° (for the cases of 1-1 and 2-1).

For the magnification effects, a set of iterative analyses have been performed in order to assess the true motion amplitudes according to Se. 2-4-4. The details are not presented here for brevity but the drift time history response at VVS B (second balcony level) is verified with comparison to the outputs from the accelerometer installed in the same location. It is necessary to mention that since the acceleration records are the direct output signals measured by the accelerometer, a numerical double integration were performed on these signals to obtain displace-

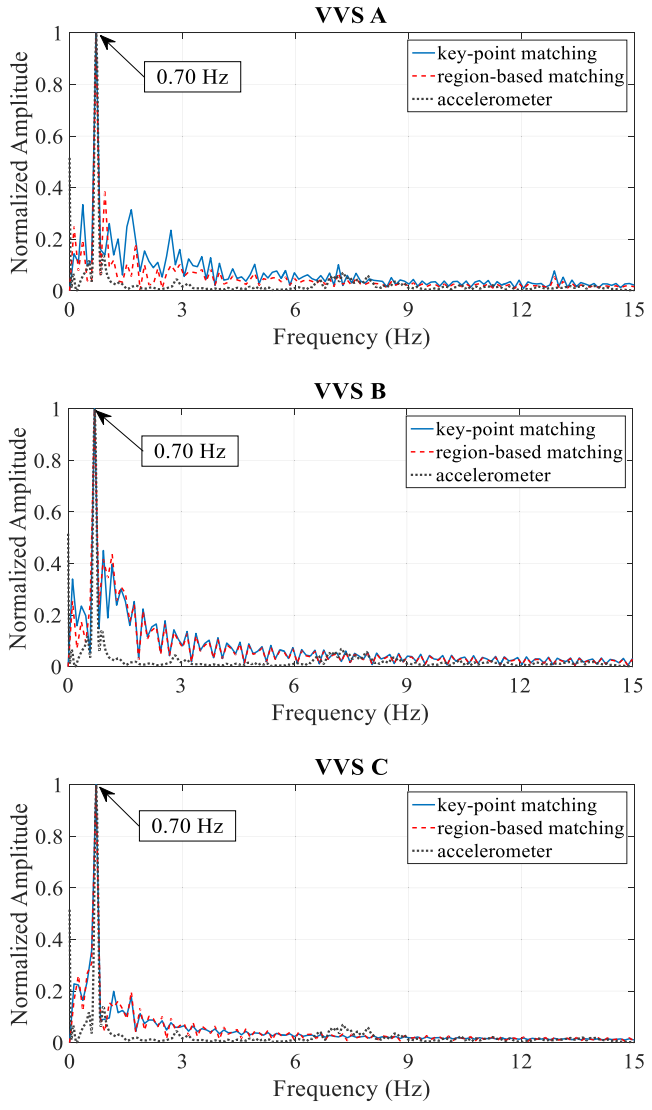

Fig. 19. The frequency spectra of the output motion signal of case 1-1.

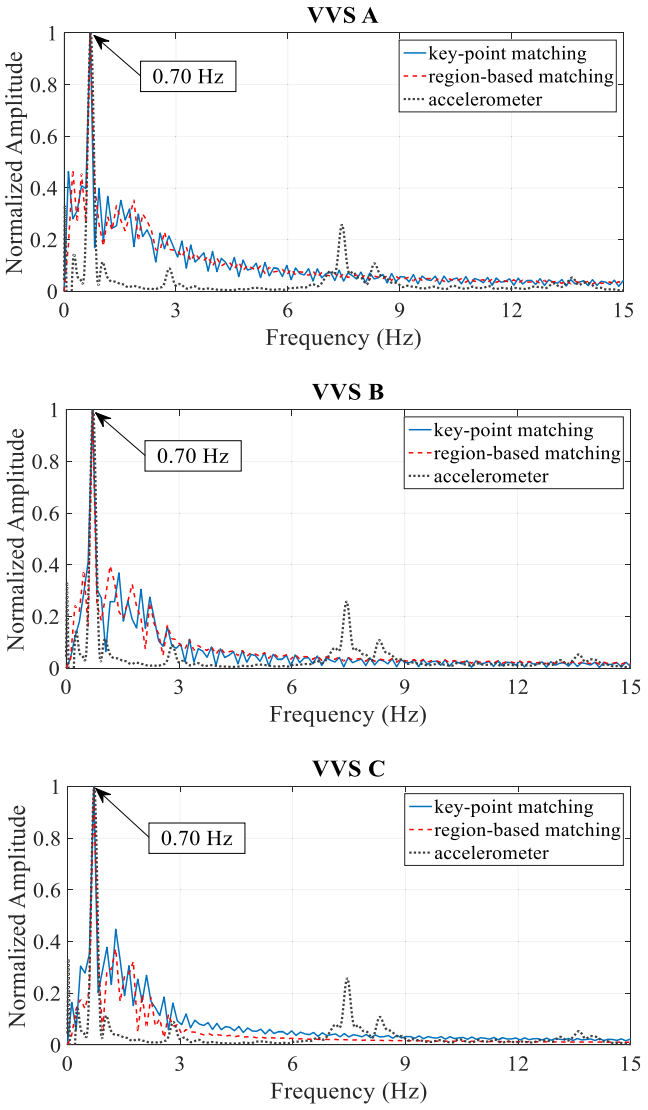

Fig. 20. The frequency spectra of the output motion signal of case 1-2.

ment responses from the acceleration records using the following equation:

$$\left.\begin{aligned} V_j^a &= V_{j-1}^a + A_j^a dt^{`} \\ D_j^a &= D_{j-1}^a + V_j^a dt^{`} \end{aligned}\right\} \rightarrow D_j^a = D_{j-1}^a + V_{j-1}^a dt^{`} + A_j^a dt^{`2} \quad (j = 1, 2, \cdots, NF^a) \tag{13}$$

In this equation, D_j^a, V_j^a and A_j^a are the intended horizontal or vertical component of displacement, velocity and acceleration values, respectively at j^{th} accelerometer recording step. Thus, D_{j-1}^a and V_{j-1}^a are the same values corresponded to the $(j-1)^{th}$ recording step. $dt^{`}$ is the time step of accelerometer data recording. A zero initial conditions ($D_0^a = 0$& $V_0^a = 0$) is also assumed to solve these numerical equations. NF^a is the total number of the accelerometer data recorded simultaneously with the camera video recording duration. These two displacement time history outputs are now comparable. The comparison is presented in Fig. 22 for the cases of 1-2 and 2-1 corresponded to the dominant wind direction using key-point matching approach.

The results presented in this figure (obtained from VVS B and the accelerometer) are generally similar. The maximum values of displacement response in all cases have been shown in Table 3. As can be seen from the table, the high-amplitude vibrations of the minarets 1 and 2 are respectively corresponded to axes 2 and 1, as expected parallel to the dominant wind direction. Also, the accuracy of the proposed video-based indirect measurement procedure using key-point matching approach is acceptable in assessment of the maximum displacement response, unlike the other approach. In the region-based approach, it seems that the motion signal averaging between key-point pixel (as a moving pixel on the boundary) and its neighbor pixels (especially those located outside the boundary as stationary pixels) leads to significantly reduced amplitude of response and consequently less accuracy.

Table 2
The determined experimental damping ratios of the investigated minarets.

Case	ξ^{exp} (%)						
	VVS A		*VVS B*		*VVS C*		*Accelerometer*
	KP	*RB*	*KP*	*RB*	*KP*	*RB*	
1-1	5.4	5.1	5.4	6.4	6.5	6.2	5.6
1-2	7.0	7.4	7.6	6.2	6.8	6.8	6.5
2-1	6.0	7.7	6.6	5.8	5.6	5.5	6.2
2-2	6.2	7.3	6.8	6.7	5.9	5.7	6.1

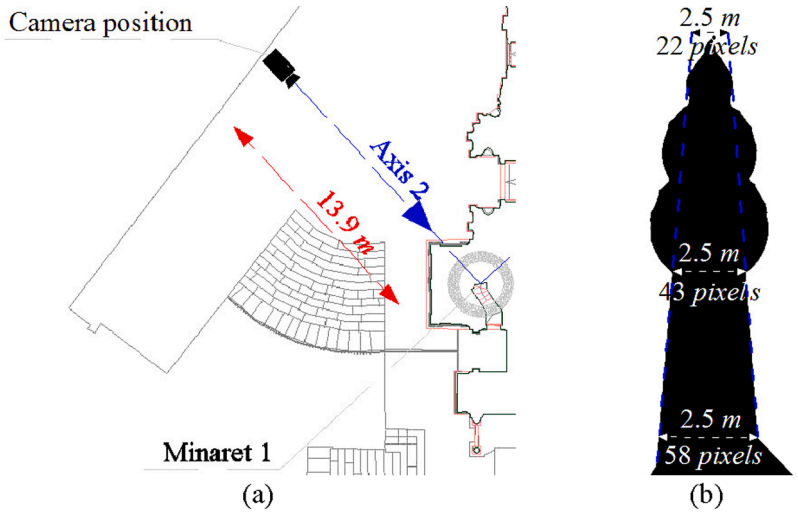

Fig. 21. (a) The camera distance to minaret 1 and (b) the perspective effect in the view from axis 2.

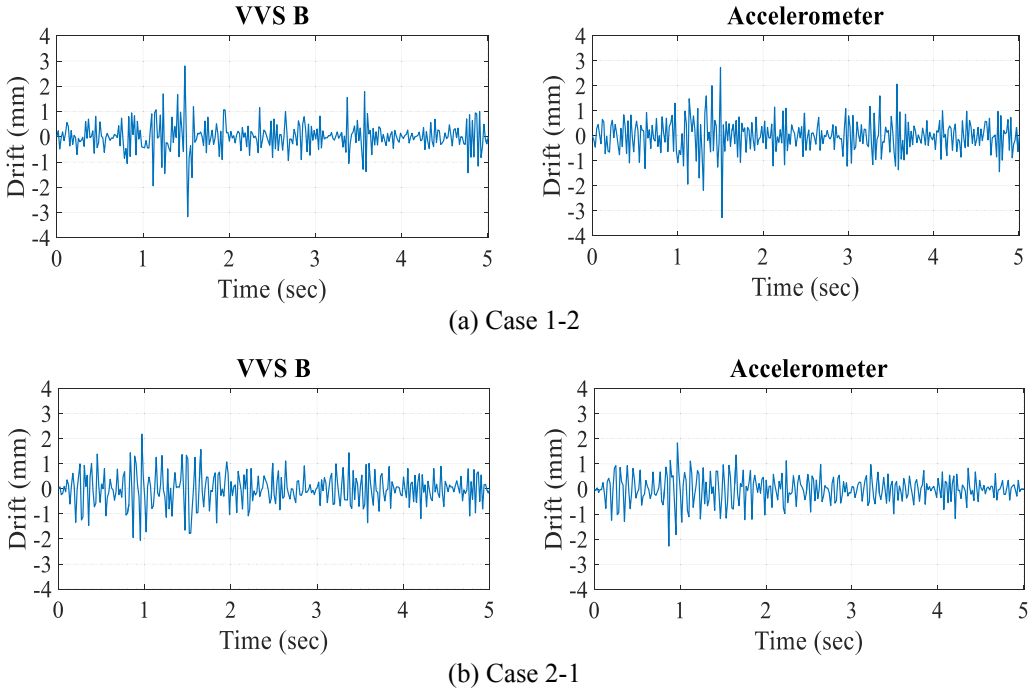

Fig. 22. Calculated lateral drift time histories of VVS B and the accelerometer.

Table 3
The peak values of minarets lateral drift at the second balcony level (in mm).

Case	*VVS B*		*Accelerometer*
	Key-Point Matching	*Region-Based Matching*	
1-1	0.3	0.2	0.2
1-2	3.3	1.6	3.2
2-1	2.2	1.2	2.3
2-2	0.1	0.1	0.1

4. Conclusion

In this study, a new step-by-step video-based indirect measurement procedure has been presented that is able to remove usual limitations on real-time SHM projects. The developed procedure utilizes a novel PMP-based (Pre-modification, Magnification and Post-modification) video conversion process in order to modify the input motion videos which have not appropriate conditions. The main outputs of this process are converted high-quality and well-conditioned videos which can be used for digital signal and image processing analyses. The signal and video processing step of the converted video records is conducted using virtual visual sensor technology. In the following of this research, an example of application including the field-measurements of historic minarets of Nur-u Osmaniye Mosque in Istanbul has been presented. The final results of the investigated minarets were verified by comparison with the outputs of an installed accelerometer sensor. Some of the main obtained observations are:

- The Eulerian video magnification process generates high-level of noises around the vibrating object. But the modification steps are able to significantly eliminate these noises.

- The PMP process is powerful and effective in production of accurate motion frequency spectrums having low-amplitude noises. Also, the examined indirect VVS-based method is able to accurately detect the experimental modal frequency, damping ratio and lateral drift time history response of the minarets in comparison of accelerometer data. These promising observations were experienced using a very simple and low-cost camera under inappropriate environmental and unpleasant weather conditions.
- It is not required that high resolution video records are prepared for this procedure. The initial size of recorded videos can be significantly reduced and the required video processing steps can be conducted with considerable saving in analysis time and data size.
- The region-based approach leads to underestimate results in drift time history responses. Accordingly, it seems that key-point matching should be considered as default approach in VVS-based digital motion signal processing investigations.

In this research the efficiency and accuracy of this proposed step-by-step camera-based indirect measurement procedure was investigated. As a limitation in the present form, it utilizes complicated algorithms in its magnification and digital video processing steps that may not be user-friendly for engineers in SHM projects. For this reason, it is suggested that a new comprehensive software package is developed in such a way that all implementation steps from PMP-based video conversion to subsequent VVS-based digital signal and image processing can be performed in one GUI. Also some other suggestions for the next studies can be offered:

- Similar studies are performed more completely. For example, development of full numerical models of the monitored structure is helpful. Such models can be constructed intactly or with presence of crack/gap elements on the structural body representing possible damages. Such numerical models can be useful for verification purposes.
- The frequency modal shapes of monitored structure are quantitatively extracted using this VVS-based measurement procedure. The procedure has no limitation in this regard. Therefore, if a sensor network with sufficient number of accelerometers or strain-gauge devices is used, the modal shapes can be experimentally verified in comparison with sensor network outputs.
- In this study, the experimental results of the proposed procedure were compared to accelerometer sensor outputs as the intended versification method. Such an investigation can be progressed by further comparisons in the next related research works using outputs of other methods or measurement devices.

CRediT authorship contribution statement

M. Ghandil: Methodology, Software, Validation, Formal analysis, Investigation, Data curation, Writing - original draft, Visualization. **Ö. Dabanli:** Validation, Resources, Data curation, Writing - review & editing, Supervision. **H. Tajmir Riahi:** Conceptualization, Writing - review & editing, Supervision, Project administration.

Declaration of Competing Interest

The authors declare that they have no known competing financial interests or personal relationships that could have appeared to influence the work reported in this paper.

Acknowledgement

This research was supported by FSMVÜ KURAM within the *Video-based Structural System Identification of Historic Structures Project* (*EVM-HIST-19*) in the scope of EU's support for education, training, youth, and sport in KA107 ERASMUS+ programme for academic year 2019/2020 (ID code: TR ISTANBU39).

References

[1] H. Sohn, C.R. Farrar, F.M. Hemez, D.D. Shunk, D.W. Stinemates, B.R. Nadler, J. J. Czarnecki, A review of structural health monitoring literature: 1996–2001, Los Alamos National Laboratory, USA, 2003.
[2] F. Casciati, M. Giordano, Fifth European Workshop on Structural Health Monitoring 2010, DEStech Publications Inc., 2010.
[3] F. Moschas, S. Stiros, Measurement of the dynamic displacements and of the modal frequencies of a short-span pedestrian bridge using GPS and an accelerometer, Eng. Struct. 33 (1) (2011) 10–17.
[4] F. Moreu, H. Jo, J. Li, R.E. Kim, S. Cho, A. Kimmle, S. Scola, H. Le, B. Spencer Jr, J. M. LaFave, Dynamic assessment of timber railroad bridges using displacements, J. Bridge Eng. 20 (10) (2015) 04014114.
[5] J.R. Gaxiola-Camacho, R. Bennett, G.M. Guzman-Acevedo, I.E. Gaxiola-Camacho, Structural evaluation of dynamic and semi-static displacements of the Juarez Bridge using GPS technology, Measurement 110 (2017) 146–153.
[6] J. dos Reis, C. Oliveira Costa, J. Sá da Costa, Strain gauges debonding fault detection for structural health monitoring, Struct. Control Health Monit. 25 (12) (2018), e2264.
[7] T. Khuc, T.A. Nguyen, H. Dao, F.N. Catbas, Swaying Displacement Measurement for Structural Monitoring Using Computer Vision and an Unmanned Aerial Vehicle, Measurement (2020) 107769.
[8] R. Calcada, A. Cunha, R. Delgado, Dynamic analysis of metallic arch railway bridge, J. Bridge Eng. 7 (4) (2002) 214–222.
[9] C.C. Spyrakos, I.G. Raftoyiannis, J.C. Ermopoulos, Condition assessment and retrofit of a historic steel-truss railway bridge, J. Constr. Steel Res. 60 (8) (2004) 1213–1225.
[10] A. Brencich, D. Sabia, Experimental identification of a multi-span masonry bridge: The Tanaro Bridge, Constr. Build. Mater. 22 (10) (2008) 2087–2099.
[11] L.F. Ramos, L. Marques, P.B. Lourenço, G. De Roeck, A. Campos-Costa, J. Roque, Monitoring historical masonry structures with operational modal analysis: two case studies, Mech. Syst. Sig. Process. 24 (5) (2010) 1291–1305.
[12] İ. Çalık, A. Bayraktar, T. Türker, H. Karadeniz, Structural dynamic identification of a damaged and restored masonry vault using Ambient Vibrations, Measurement 55 (2014) 462–472.
[13] B. Jaishi, W.-X. Ren, Z.-H. Zong, P.N. Maskey, Dynamic and seismic performance of old multi-tiered temples in Nepal, Eng. Struct. 25 (14) (2003) 1827–1839.
[14] F. Casarin, C. Modena, Seismic assessment of complex historical buildings: application to Reggio Emilia Cathedral, Italy, Int. J. Architec. Heritage 2 (3) (2008) 304–327.
[15] A. Pau, F. Vestroni, Vibration analysis and dynamic characterization of the Colosseum, Struct. Control Health Monit. Off. J. Int. Assoc. Struct. Control Monit. Eur. Assoc. Control Struct. 15 (8) (2008) 1105–1121.
[16] A. De Stefano, E. Matta, P. Clemente, Structural health monitoring of historical heritage in Italy: some relevant experiences, J. Civ. Struct. Health Monit. 6 (1) (2016) 83–106.
[17] A. Altunisik, E. Kalkan, F. Okur, K. Ozgan, O. Karahasan, A. Bostanci, Non-destructive modal parameter identification of historical timber bridges using ambient vibration tests after restoration, Measurement 146 (2019) 411–424.
[18] D.-H. Yang, T.-H. Yi, H.-N. Li, Y.-F. Zhang, Correlation-based estimation method for cable-stayed bridge girder deflection variability under thermal action, J. Perform. Constr. Facil 32 (5) (2018) 04018070.
[19] T. Tang, D.-H. Yang, L. Wang, J.-R. Zhang, T.-H. Yi, Design and application of structural health monitoring system in long-span cable-membrane structure, Earthquake Eng. Eng. Vibr. 18 (2) (2019) 461–474.
[20] F. Aras, L. Krstevska, G. Altay, L. Tashkov, Experimental and numerical modal analyses of a historical masonry palace, Constr. Build. Mater. 25 (1) (2011) 81–91.
[21] L.F. Ramos, R. Aguilar, P.B. Lourenço, Operational modal analysis of historical constructions using commercial wireless platforms, Struct. Health Monit. 10 (5) (2011) 511–521.
[22] S. Bennati, L. Nardini, W. Salvatore, Dynamical behaviour of a masonry medieval tower subjected to bell's action. Part I: bell's action measurement and modelling, 2005.
[23] S. Bennati, L. Nardini, W. Salvatore, Dynamical behaviour of a masonry medieval tower subjected to bell's action. Part II: measurement and modelling of the tower motion, 2005.
[24] C. Gentile, A. Saisi, Ambient vibration testing of historic masonry towers for structural identification and damage assessment, Constr. Build. Mater. 21 (6) (2007) 1311–1321.
[25] S. Ivorra, F.J. Pallarés, Dynamic investigations on a masonry bell tower, Eng. Struct. 28 (5) (2006) 660–667.
[26] K.A. Bani-Hani, H.S. Zibdeh, K. Hamdaoui, Health monitoring of a historical monument in Jordan based on ambient vibration test, Smart Struct. Syst 4 (2) (2008) 195–208.
[27] F. Peña, P.B. Lourenço, N. Mendes, D.V. Oliveira, Numerical models for the seismic assessment of an old masonry tower, Eng. Struct. 32 (5) (2010) 1466–1478.
[28] C. Oliveira, E. Çaktı, D. Stengel, M. Branco, Minaret behavior under earthquake loading: The case of historical Istanbul, Earthquake Eng. Struct. Dyn. 41 (1) (2012) 19–39.
[29] D. Foti, M. Diaferio, N.I. Giannoccaro, M. Mongelli, Ambient vibration testing, dynamic identification and model updating of a historic tower, NDT E Int. 47 (2012) 88–95.

[30] C. Gentile, A. Saisi, A. Cabboi, Structural identification of a masonry tower based on operational modal analysis, Int. J. Architec. Heritage 9 (2) (2015) 98–110.
[31] R. Ceravolo, G. Pistone, L.Z. Fragonara, S. Massetto, G. Abbiati, Vibration-based monitoring and diagnosis of cultural heritage: a methodological discussion in three examples, Int. J. Architec. Heritage 10 (4) (2016) 375–395.
[32] F. Ubertini, G. Comanducci, N. Cavalagli, Vibration-based structural health monitoring of a historic bell-tower using output-only measurements and multivariate statistical analysis, Struct. Health Monit. 15 (4) (2016) 438–457.
[33] J.G. Chen, A. Davis, N. Wadhwa, F. Durand, W.T. Freeman, O. Büyüköztürk, Video camera–based vibration measurement for civil infrastructure applications, J. Infrastruct. Syst. 23 (3) (2016) B4016013.
[34] J.G. Chen, N. Wadhwa, Y.-J. Cha, F. Durand, W.T. Freeman, O. Buyukozturk, Modal identification of simple structures with high-speed video using motion magnification, J. Sound Vib. 345 (2015) 58–71.
[35] J.G. Chen, N. Wadhwa, F. Durand, W.T. Freeman, O. Buyukozturk, Developments with motion magnification for structural modal identification through camera video, in Dynamics of Civil Structures vol. 2 (2015) 49–57.
[36] M. Elgharib, M. Hefeeda, F. Durand, W.T. Freeman, Video magnification in presence of large motions. Proceedings of the IEEE Conference on Computer Vision and Pattern Recognition, 2015.
[37] L. Liu, L. Lu, J. Luo, J. Zhang, X. Chen, Enhanced Eulerian video magnification. 2014 7th International Congress on Image and Signal Processing, IEEE, 2014.
[38] Z. Shang, Z. Shen, Multi-point vibration measurement for mode idetification of bidge sructures using vdeo-based mtion magnification, 2017. arXiv preprint arXiv: 1712.06566.
[39] Z. Shang, Z. Shen, Multi-point vibration measurement and mode magnification of civil structures using video-based motion processing, Autom. Constr. 93 (2018) 231–240.
[40] N. Wadhwa, M. Rubinstein, F. Durand, W.T. Freeman, Phase-based video motion processing, ACM Trans. Graphics 32 (4) (2013) 80.
[41] N. Wadhwa, H.-Y. Wu, A. Davis, M. Rubinstein, E. Shih, G.J. Mysore, J.G. Chen, O. Buyukozturk, J.V. Guttag, W.T. Freeman, Eulerian video magnification and analysis, Commun. ACM 60 (1) (2016) 87–95.
[42] H.-Y. Wu, M. Rubinstein, E. Shih, J. Guttag, F. Durand, W. Freeman, Eulerian video magnification for revealing subtle changes in the world, ACM Trans. Graphics 31 (4) (2012) 1–8.
[43] D. Zhang, L. Fang, Y. Wei, J. Guo, B. Tian, Structural low-level dynamic response analysis using deviations of idealized edge profiles and video acceleration magnification, Appl. Sci. 9 (4) (2019) 712.
[44] Y. Zhang, S.L. Pintea, J.C. Van Gemert, Video acceleration magnification. Proceedings of the IEEE Conference on Computer Vision and Pattern Recognition, 2017.
[45] M. Zimmermann, U. Gülan, Y.E. Harmanci, E.N. Chatzi, M. Holzner, Structural health monitoring through video recording. Proceedings of the 8th European Workshop On Structural Health Monitoring (EWSHM 2016), Bilbao, Spain, 2016.
[46] A.J. Choi, J.-H. Han, Frequency-based damage detection in cantilever beam using vision-based monitoring system with motion magnification technique, J. Intell. Mater. Syst. Struct. 29 (20) (2018) 3923–3936.
[47] D. Feng, M.Q. Feng, Experimental validation of cost-effective vision-based structural health monitoring, Mech. Syst. Sig. Process. 88 (2017) 199–211.
[48] A. Havaran, M. Mahmoudi, Extracting structural dynamic properties utilizing close photogrammetry method, Measurement 150 (2020), 107092.
[49] A. Havaran, M. Mahmoudi, Markers tracking and extracting structural vibration utilizing Randomized Hough transform, Autom. Constr. 116 (2020), 103235.
[50] A. Shariati, T. Schumacher, N. Ramanna, Eulerian-based virtual visual sensors to detect natural frequencies of structures, J. Civ. Struct. Health Monit. 5 (4) (2015) 457–468.
[51] V. Fioriti, I. Roselli, A. Tatì, G. De Canio, Historic masonry monitoring by motion magnification analysis, WIT Trans. Ecol. Environ. 223 (2017) 367–375.
[52] T. Gautama, M. Van Hulle, A phase-based approach to the estimation of the optical flow field using spatial filtering, IEEE Trans. Neural Networks 13 (5) (2002) 1127–1136.
[53] C. Liu, A. Torralba, W.T. Freeman, F. Durand, E.H. Adelson, Motion magnification, ACM Trans. Graphics (TOG) 24 (3) (2005) 519–526.
[54] S. Patsias, W. Staszewskiy, Damage detection using optical measurements and wavelets, Struct. Health Monit. 1 (1) (2002) 5–22.
[55] Y.-Z. Song, C.R. Bowen, A.H. Kim, A. Nassehi, J. Padget, N. Gathercole, Virtual visual sensors and their application in structural health monitoring, Struct. Health Monit. 13 (3) (2014) 251–264.
[56] J.T. Scheick, Linear algebra with applications, vol. 81, McGraw-Hill New York, 1997.
[57] S. Lang, Introduction to linear algebra, Springer Science & Business Media, 2012.
[58] T. Schumacher, A. Shariati, Monitoring of structures and mechanical systems using virtual visual sensors for video analysis: Fundamental concept and proof of feasibility, Sensors 13 (12) (2013) 16551–16564.
[59] B.D. Lucas, T. Kanade, Optical navigation by the method of differences, IJCAI, Citeseer, 1985.
[60] B. Lucas, T. Kanade, Performance of optical flow techniques. Proc DARPA IU Workshop, 1981.
[61] B. Lucas, T. Kanade, Detection and tracking of point features. Technical Report MU CS 91 132 Carnegie Mellon University, 1991.
[62] MathWorks, MATLAB R2018b (Computer programming language), Natick, MA, 2018.
[63] O. Dabanli, Operational modal analysis of Nur-uosmaniye mosque in Istanbul, in: 7th International Operational Modal Analysis Conference: Ingolstadt, Germany, 2017.
[64] O. Dabanli, Determination of earthquake performance of Nuruosmaniye Mosque and conservation proposals (PhD Thesis), Istanbul Technical University, Institute of Science, Istanbul, TR, 2016.
[65] Meteoblue. Weather Istanbul [Jan 17, 2020]; Available from: http://www.meteoblue.com.
[66] E.L. Wilson, A. Habibullah, SAP2000 18: integrated finite element analysis and design of structures, Computers and Structures, Berkeley, California., 2017.
[67] A.K. Chopra, Dynamics of Structures: Theory and Applications to Earthquake Engineering, fourth ed., Pearson Education Inc., Prentice Hall, NJ, 2012.